The Journal of Chemical Physics

Kinetic pathways of water exchange in the first hydration shell of magnesium: Influence of water model and ionic force field

Cite as: J. Chem. Phys. **155**, 084503 (2021); https://doi.org/10.1063/5.0060896
Submitted: 23 June 2021 • Accepted: 09 August 2021 • Published Online: 25 August 2021

Sebastian Falkner and Nadine Schwierz

View Online Export Citation CrossMark

ARTICLES YOU MAY BE INTERESTED IN

Kinetic pathways of water exchange in the first hydration shell of magnesium
The Journal of Chemical Physics **152**, 224106 (2020); https://doi.org/10.1063/1.5144258

Machine learning implicit solvation for molecular dynamics
The Journal of Chemical Physics **155**, 084101 (2021); https://doi.org/10.1063/5.0059915

Software for the frontiers of quantum chemistry: An overview of developments in the Q-Chem 5 package
The Journal of Chemical Physics **155**, 084801 (2021); https://doi.org/10.1063/5.0055522

© 2021 Author(s).

The Journal of Chemical Physics ARTICLE scitation.org/journal/jcp

Kinetic pathways of water exchange in the first hydration shell of magnesium: Influence of water model and ionic force field

Cite as: J. Chem. Phys. 155, 084503 (2021); doi: 10.1063/5.0060896
Submitted: 23 June 2021 • Accepted: 9 August 2021 •
Published Online: 25 August 2021

View Online Export Citation CrossMark

Sebastian Falkner[1] and Nadine Schwierz[2,a)]

AFFILIATIONS

[1] Faculty of Physics, University of Vienna, 1090 Vienna, Austria
[2] Department of Theoretical Biophysics, Max Planck Institute of Biophysics, 60438 Frankfurt am Main, Germany

[a)] **Author to whom the correspondence should be addressed:** nadine.schwierz@biophys.mpg.de

ABSTRACT

Water exchange between the first and second hydration shell is essential for the role of Mg^{2+} in biochemical processes. In order to provide microscopic insights into the exchange mechanism, we resolve the exchange pathways by all-atom molecular dynamics simulations and transition path sampling. Since the exchange kinetics relies on the choice of the water model and the ionic force field, we systematically investigate the influence of seven different polarizable and non-polarizable water and three different Mg^{2+} models. In all cases, water exchange can occur either via an indirect or direct mechanism (exchanging molecules occupy different/same position on the water octahedron). In addition, the results reveal a crossover from an interchange dissociative (I_d) to an associative (I_a) reaction mechanism dependent on the range of the Mg^{2+}–water interaction potential of the respective force field. Standard non-polarizable force fields follow the I_d mechanism in agreement with experimental results. By contrast, polarizable and long-ranged non-polarizable force fields follow the I_a mechanism. Our results provide a comprehensive view on the influence of the water model and the ionic force field on the exchange dynamics and the foundation to assess the choice of the force field in biomolecular simulations.

© 2021 Author(s). All article content, except where otherwise noted, is licensed under a Creative Commons Attribution (CC BY) license (http://creativecommons.org/licenses/by/4.0/). https://doi.org/10.1063/5.0060896

INTRODUCTION

In aqueous solutions, Mg^{2+} ions are surrounded by a hydration shell of six water molecules, which is subsequently enclosed by a second hydration shell. Water exchange between these hydration shells plays an important role in a large variety of biochemical processes ranging from simple ion pair formation to catalyzed reactions in metalloenzymes or the transport of ions across cell membranes.[1–5] Since water exchange governs any type of reaction involving the replacement of the strongly bound hydration water molecules, resolving the reaction mechanism has received considerable scientific attention in experiments and simulations.[6–13]

Experimental techniques such as dielectric relaxation, x-ray adsorption, femtosecond mid-infrared, and far-infrared adsorption spectroscopy provide insight into the solvation structure of Mg^{2+},[2,14–16] while nuclear magnetic resonance (NMR) experiments facilitate the direct measurement of water exchange rates.[6–8] However, the structural changes during water exchange are experimentally not directly accessible. Still, according to the mechanistic classification for ligand exchange reactions proposed by Langford and Gray,[17] the mechanism can be divided into four categories: associative (A), dissociative (D), interchange associative (I_d), and interchange dissociative (I_a). In the former two categories, a detectable intermediate with increased (A) or decreased (D) coordination number exists. For the latter two categories, no kinetically detectable intermediate exists. In order to discriminate between the four categories, the activation volume is typically used for the experimental identification of the water exchange mechanism.[7,18] In general, the activation volume is defined as the difference between the partial molar volume of the reactants and that of the transition state at a given temperature and is typically derived from the pressure dependence of the observed rate constant of a chemical reaction in experiments. The observed exchange rate is either slowed or accelerated by increasing the pressure, leading to a positive or negative sign of the activation volume, respectively. In solvent exchange reactions, a positive activation volume indicates elongated

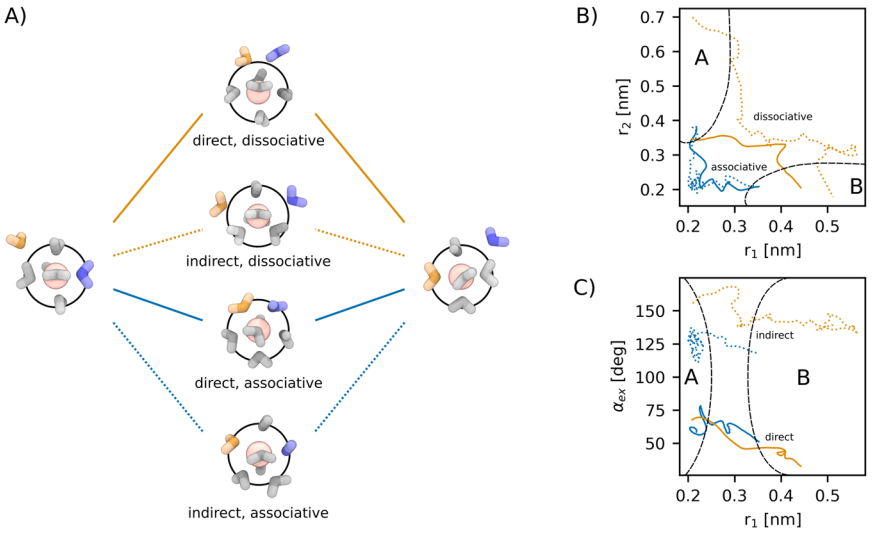

FIG. 1. Overview of the observed exchange mechanisms for water exchange in the first hydration shell of Mg^{2+}. (a) Simulation snapshots of the two stable states and the transition states for the spectrum of water exchange processes. Black circles indicate the size of the first hydration shell. (b) Four representative pathways connecting the two stable states as a function of the distance of the exchanging water molecules, r_1 and r_2. In this representation, associative and dissociative pathways are clearly separated. (c) Pathways as function of r_1 and the exchange angle α_{ex} showing a clear separation of the direct and indirect exchange mechanism.

distances and angles of the exchanging molecules in the transition state.[7] Here, the exchange occurs outside of the first hydration shell, and the mechanism is classified as dissociative. A negative activation volume reflects that the distances and angles are reduced, the exchange occurs inside the first hydration shell, and the mechanism is classified as associative.[7]

For Mg^{2+}, the activation volume is positive, and based on the similarity with Co^{2+} and Ni^{2+}, the I_d or D mechanism has been proposed.[7,8] However, the question, which mechanism is dominant could not be settled with certainty.[8]

Here, simulations could provide further insights by a unique atomistic description of the exchange dynamics. However, simulating water exchange is tremendously challenging for two reasons. (i) Water exchange around Mg^{2+} is rare. According to experiments, water exchange is on the microsecond timescale.[6–8] Therefore, straightforward simulations are unsuitable to sample water exchange with sufficient statistics. (ii) Water exchange involves the concerted motion of several water molecules. The water molecules exchange in a concerted fashion, and the molecules in the first hydration shell and beyond rearrange collectively.[12] Consequently, *ab initio* quantum mechanical calculations are not feasible to resolve the exchange dynamics due to their high computational costs and limited system size. On the other hand, classical all-atom simulations in combination with transition path sampling have proven to be a particularly powerful sampling strategy to resolve the molecular exchange pathways.[12] In agreement with the experimental results, the simulations revealed an interchange dissociative exchange process. In addition, two alternative exchange pathways were resolved. In the transition states of the indirect pathways, the entering and leaving water molecules enter on opposite sides of the water octahedron, leading to an exchange angle of ~124° [Fig. 1(a), direct, dissociative]. In the direct exchange mechanism, the exchange takes place via the attack of the incoming water molecule onto one edge of the water octahedron, and the resulting exchange angle is ~53° [Fig. 1(a), indirect, dissociative].

In general, simulations rely on the accuracy of the available water and Mg^{2+} force fields. In particular, different water models and ionic force fields can have significant effects on the structural, thermodynamic, and kinetic properties.[10,13,19,20] For example, the rate of water exchange in the first hydration shell of Mg^{2+} varies by more than eight orders of magnitude depending on the exact choice of the force field.[10,13] The choice of the water model and the ionic force field is therefore crucial to yield a quantitative description of Mg^{2+} in biomolecular simulations. In particular, capturing the mechanism of ligand exchange is essential to describe the role of Mg^{2+} in biochemical processes.

In order to assess the choice of different force fields in biomolecular simulations involving Mg^{2+}, we here systematically investigate the influence of seven different polarizable and non-polarizable water and three different Mg^{2+} models. Using all-atom molecular dynamics (MD) simulations in combination with transition path sampling, we cover the long timescales involved and resolve the kinetic pathways. The results provide comprehensive insights into the influence of the water model and the ionic force field on the exchange mechanism.

METHODS

Atomistic model and simulation setup

The systems consist of one Mg^{2+} ion and 506 water molecules in a cubic simulation box (L = 25 Å). We used three different polarizable and non-polarizable Mg^{2+} force fields and seven different water models as described below.

For the non-polarizable systems, the simulations were performed using Gromacs 2018.8.[21] Long-range electrostatic interactions were accounted for using particle-mesh Ewald summation with a Fourier spacing of 0.12 nm and a grid interpolation up to order 4. Short-range Coulomb and Lennard-Jones (LJ) interactions were cut off at 1.2 nm. Long-range dispersion corrections for energy and pressure were applied to correct for the truncated LJ potential. Prior to transition path sampling, the systems were minimized using the steepest descent algorithm. An NVT and NPT equilibration was performed each for 1 ns. All path sampling simulations were

© Author(s) 2021

performed in the NVT ensemble at a temperature of 300 K with a time step of 2 fs using the velocity rescaling thermostat with a stochastic term.[22]

For the polarizable systems, the simulations were performed in OpenMM 7.4.1.[23] Short-range Coulomb and Lennard-Jones (LJ) interactions were cut off at 1.2 nm. Long-range electrostatic interactions were treated using particle-mesh Ewald summation. Simulations were performed with mutual polarization using the convergence criteria of 10^{-5} D. Trial trajectories were generated using the velocity Verlet with a velocity randomization integrator[24] from the OpenMMTools library[25] at 300 K with a time step of 0.5 fs.

Mg^{2+} force fields

We used three different Mg^{2+} force fields: the non-polarizable Mg^{2+} by Mamatkulov and Schwierz,[20] the microMg parameters,[13] and the polarizable Mg^{2+} parameters[26,27] from the AMOEBA-2013 force field.[28,29] The Mamatkulov Mg^{2+} parameters were optimized in our previous work[20] to reproduce the experimental solvation free energy and the activity derivative. To test the influence of the water, we here used the Mamatkulov Mg^{2+} parameters in combination with six different non-polarizable water models, described in the corresponding section of the manuscript. In addition, we used the microMg parameters in combination with the TIP3P water model. The microMg parameters were optimized in our most recent work[13] to reproduce the experimental water exchange rate in addition to the before-mentioned thermodynamic properties. Finally, we used the polarizable AMOEBA force field[28,29] with the optimized Mg^{2+} parameters[26,27] to explicitly account for the polarizability of Mg^{2+} and water.

Water models

We used seven different non-polarizable and polarizable water models. From the different three-site models, we chose the two most commonly used models, namely, the SPC/E[30] and the TIP3P[31] water models. From the different four-site models, we chose TIP4P/2005[32] and TIP4P-D.[33] TIP4P/2005 has gained popularity and is often quoted as the best non-polarizable general-purpose model.[34] TIP4P-D is one of the newer offsprings in the TIP4P family and was designed to improve water dispersion interactions. From the different five-site models, we chose TIP5P-E[35] and TIP5P/2018.[36] TIP5P-E is the re-parameterized version of the original TIP5P model[37] for use with Ewald summation methods. Since the TIP5P water model has not performed up to the initial expectations,[34] we also used the TIP5P/2018 water model due to its improved bulk properties and its expected good performance in biomolecular simulations. As a polarizable water model, the AMOEBA water model[28,29] was used.

Transition path sampling and transition state ensemble

Transition path sampling in the non-polarizable system was performed using OpenPathSampling[38,39] with Gromacs 2018.8.[21] An initial path was created using constant force pulling along the Mg^{2+}–O_w distance using PLUMED.[40] New trial trajectories were created by selection of a snapshot, velocity randomization, and integration forward and backward in time. For path sampling with Mg^{2+} parameters from Mamatkulov and Schwierz,[20] the shooting point selection was biased along the Mg^{2+}–O_w distance with respect to the leaving water molecule using a Gaussian centered at 0.325 nm and a width of 150 nm^{-2}.[41] The path length was flexible, and the integration stopped when a stable state was reached. The states were defined based on the Mg^{2+}–O_w distance with respect to the leaving water molecule. Additionally, the number of water oxygen atoms in the inner shell with a cutoff of 0.21 nm was included to ensure that Mg^{2+} is coordinated by six water molecules in the stable states.

In the polarizable system, transition path sampling was performed using OpenPathSampling[38,39] with OpenMM 7.4.1.[23] Here, the initial path was generated at high temperature. As in the non-polarizable setup, new trial trajectories were generated by two-way shooting with randomized velocities. In contrast, it was not necessary to impose a bias on the snapshot selection. As previously mentioned, the stable states were defined based on the Mg^{2+}–O_w distance with respect to the leaving water molecule. Due to the different exchange mechanism (I_a), the number of water oxygen atoms within a cutoff of 0.35 nm was used to ensure Mg^{2+} is coordinated by six water molecules when the stable states are reached. The same state definitions were used in combination with the non-polarizable simulation protocol for the sampling of exchanges with the microMg parameters. For both non-polarizable and polarizable setups, the sampling was performed until 2500 trials were accepted.

Based on our previous work,[12] we identify transition states as configurations that fulfill the criterion $|r_1 - r_2| < 0.025$ nm. Here, the incoming and leaving water molecules are approximately equally distant from the Mg^{2+} ion and the commitment probability to either stable state is similar. While efficient to evaluate, the criterion reproduces the TIP3P transition state properties from our previous work.[12]

Activation volume calculation

The activation volume was estimated as proposed by Qian *et al.*[42] van der Waals radii of atoms involved in the exchange process were scaled by 1.186. The solvent-excluded surface formed by these atoms was modeled using NanoShaper.[43] The volume enclosed by the solvent-excluded surface was estimated using Trimesh 3.8.8. A reference volume was obtained based on a 10 ns MD simulation without any exchange events. The activation volume defined as the change of volume with respect to the reference was then calculated for all transition states.

RESULTS AND DISCUSSION

The aim of this work is to resolve how different water models and ionic force fields influence the kinetic pathways of water exchange in the first hydration shell of Mg^{2+}. In the exchange reaction, one of the six water molecules from the first hydration shell is replaced by water from the second one. To gain clear mechanistic insight, transition path sampling[44,45] is applied to obtain a large number of independent reactive pathways. The advantage of transition path sampling is that it covers the up-to-millisecond long timescales involved[6,8,12] while generating an ensemble of true dynamic trajectories free of any bias.[46] This in turn allows us to unambiguously determine the reaction mechanism with sufficient statistics.

© Author(s) 2021

Four representative pathways are shown in Fig. 1 corresponding to an associative or dissociative exchange pathway. Based on the distances between Mg^{2+} and the two exchanging water molecules, r_1 and r_2, associative and dissociative pathways are clearly distinguishable [Fig. 1(b)]. In the following, we show that the exchange occurs outside of the first hydration shell in the dissociative pathways. During activation, one water molecule from the second hydration shell enters the molecular void leading to the concerted motion of another water molecule out of the first hydration shell. The distances of the entering and leaving water molecules in the transition state are elongated, and the activation volume is positive. By contrast, in associative pathways, the exchange occurs inside the first hydration shell, the distances are shortened, and the activation volume is negative.

As shown in Fig. 1(c), the exchange can be further classified by the exchange angle between the incoming and outgoing water molecules.[12] In the indirect exchange mechanism, the entering and leaving water molecules occupy different positions on the water octahedron. In the direct exchange mechanism, the exchange takes place via an attack onto the edge of the water octahedron and the exchanging water molecules occupy the same positions on the water octahedron [Fig. 1(a)]. For instance in TIP3P, exchange angle $\alpha_{ex} < 90$ corresponds to the direct exchange mechanism while $\alpha_{ex} > 90$ corresponds to the indirect exchange mechanism [Figs. 2(b) and 2(c)].

In the following, we provide insight into the exchange pathways obtained for seven water models and three different Mg^{2+} force fields. The probability distributions of the distances and exchange angle along the reactive pathways provide direct insight into the kinetic pathways, and the regions of high probability density coincide with the transition states (Figs. 2–5, Table I).

Interchange dissociative pathways for rigid, non-polarizable, three-, four-, and five-site water models

Figures 2(a) and 2(b) show the distributions of distances and exchange angles along reactive pathways in TIP3P water. In the transition state, the distances of the leaving and entering water molecules are elongated (Table I), and the exchange takes place outside the first hydration shell. In agreement with our previous results,[12] two alternative exchange pathways, corresponding to the indirect and direct mechanism, can be clearly identified from the exchange angle [Fig. 2(b)]. In the direct exchange, the five spectator water molecules in the first hydration shell adopt a square pyramidal geometry in the transition state [Fig. 2(c)]. The indirect exchange occurs via a trigonal bipyramidal transition state. The exchanging water molecules enter and leave on opposite sides of the trigonal base [Fig. 2(c)]. This results in an exchange angle of ~120° (Table I). The activation volume is positive, and larger $r_{1,2}$ distances lead to a higher activation volume. Yet, this is not the only contributing factor. While indirect exchange reactions typically occur at smaller $r_{1,2}$ distances than direct exchange reactions, they tend to have larger activation volumes. This is likely caused by the different angular distribution of the exchanging water in the trans or cis position [Fig. 2(c)]. The distribution of transition times [Fig. 2(d)] reveals that the water molecules spend less than 1 ps in transition and the indirect exchange is, on average, slightly faster compared to the direct exchange.

In summary, the leaving water molecule departs stepwise while an incoming water is approaching. The exchanging water molecules move in a concerted fashion with no kinetically detectable intermediate characteristic of an interchange (I) mechanism. Since the intrinsic activation volume is positive, direct and indirect water exchange corresponds to an interchange dissociative (I_d) process in agreement with the experimental results.[7,8] It should be noted, however, that in equilibrium, the indirect exchange is expected to be observed much more frequently compared to the direct mechanism since conformations with cis positions of exchanging ligands (direct pathways) are energetically less favorable compared to trans positions (indirect pathway).[9]

For SPC/E, TIP4P/2005, TIP4P-D, and TIP5P/2018, the characteristics of water exchange remain essentially unchanged (Figs. 2–4). However, for SPC/E, the distribution of exchange

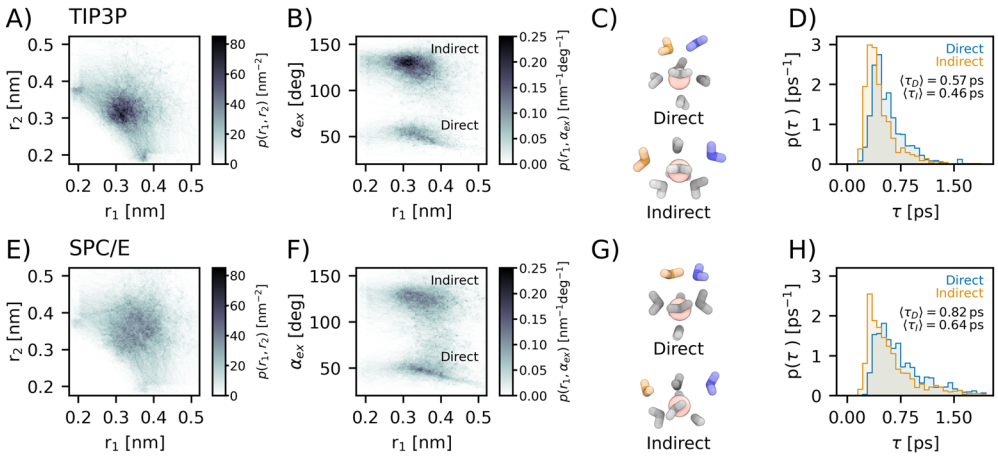

FIG. 2. Water exchange with the three-site water models TIP3P (top) and SPC/E (bottom). (a) and (e) Probability distribution function $p(r_1, r_2)$ along the transition pathways in dependence of the distances r_1 and r_2. (b) and (f) Probability distribution function $p(r_1, \alpha_{ex})$ in dependence of r_1 and the exchange angle α_{ex}. (c) and (g) Representative simulation snapshots of the transition state for the direct and indirect mechanism. (d) and (h) Distribution of transition times $p(\tau)$ for the direct and indirect exchange pathways.

© Author(s) 2021

TABLE I. Properties of the transition state ensemble for direct and indirect exchange for different water models: Mg^{2+}–oxygen distance of the exchanging water molecules, $r_{1,2}$, angle between the exchanging water oxygen atoms and Mg^{2+}, α_{ex}, average path length τ, activation volume $\Delta V^{\ddagger}$, and number N of direct and indirect exchange pathways. Averages and standard deviations of the properties are shown.

Mechanism	Model	$r_{1,2}$ (nm)	α_{ex} (deg.)	τ (ps)	$\Delta V^{\ddagger}$ (cm^3 mol^{-1})	N
Direct	TIP3P	0.342 ± 0.037	55.1 ± 9.0	0.57 ± 0.24	2.62	2 321
	SPC/E	0.372 ± 0.041	58 ± 14	0.82 ± 0.55	4.31	3 671
	TIP4P/2005	0.362 ± 0.035	54 ± 10	0.83 ± 0.34	3.54	701
	TIP4P-D	0.363 ± 0.039	56 ± 12	0.82 ± 0.42	3.62	1 974
	TIP5P-E	0.309 ± 0.019	56.5 ± 4.6	0.47 ± 0.16	1.75	1 523
	TIP5P-2018	0.341 ± 0.035	52.7 ± 7.9	0.59 ± 0.30	2.55	3 009
	microMg	0.221 ± 0.009	74.1 ± 3.5	0.96 ± 0.51	−4.88	9 389
	AMOEBA	0.235 ± 0.038	71.8 ± 7.0	0.83 ± 0.47	−4.2	6 609
Indirect	TIP3P	0.327 ± 0.033	125 ± 13	0.46 ± 0.23	2.73	8 237
	SPC/E	0.354 ± 0.039	123 ± 15	0.64 ± 0.46	4.72	7 136
	TIP4P/2005	0.331 ± 0.033	126 ± 12	0.51 ± 0.24	3.42	9 917
	TIP4P-D	0.345 ± 0.034	124 ± 14	0.65 ± 0.34	3.67	8 172
	TIP5P-E	0.303 ± 0.020	125 ± 10	0.48 ± 0.25	2.1	10 753
	TIP5P-2018	0.341 ± 0.035	125 ± 15	0.53 ± 0.28	3.89	7 685
	microMg	0.220 ± 0.010	132 ± 13	1.16 ± 0.61	−4.72	3 268
	AMOEBA	0.238 ± 0.039	138 ± 11	0.77 ± 0.45	−3.92	5 932

distances [Fig. 2(e)] is broader indicating that solvent reorientation plays a more pronounced role. This likely reflects the ideal tetrahedral shape of the SPC/E water model. Moreover, for TIP4P/2005, the indirect pathway almost completely disappears indicating that the cis position of the two exchanging water becomes less favorable [Fig. 3(b)]. The most pronounced differences are observed for TIP5P-E [Figs. 4(a) and 4(b)]. Here, the exchange takes place on the edge of the first hydration shell. The exchange distances are significantly shorter and the activation volume is smaller compared to the other water models while the exchange angles remain largely unaffected (Table I). Consequently, I_d and I_a exchange mechanisms are almost indistinguishable since bond formation and bond breaking become equally important. Here, the different angular distribution of TIP5P-E may explain the observed differences.[47] In particular, the marked difference to act as the tetrahedral hydrogen bond donor and acceptor likely leads to an interchange mechanism.

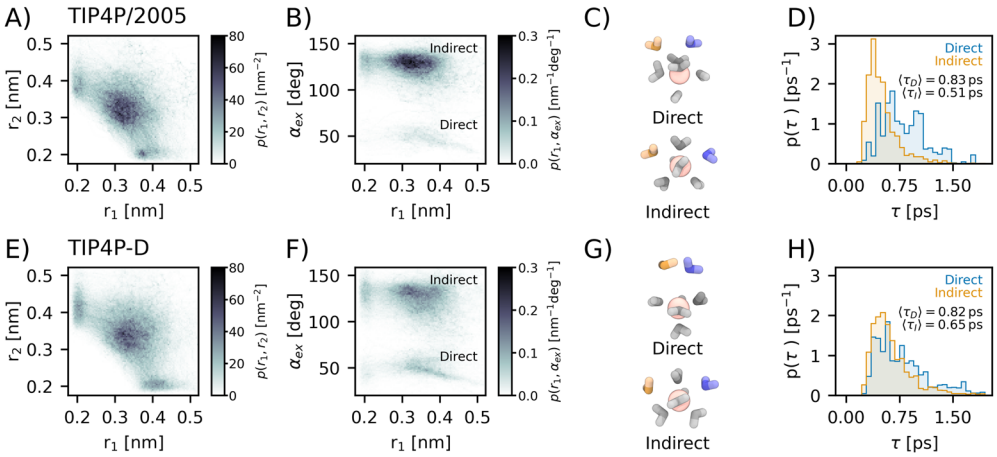

FIG. 3. Water exchange with the four-site water models TIP4P/2005 (top) and TIP4P-D (bottom). (a) and (e) Probability distribution function $p(r_1, r_2)$ along the transition pathways in dependence of the distances r_1 and r_2. (b) and (f) Probability distribution function $p(r_1, \alpha_{ex})$ in dependence of r_1 and the exchange angle α_{ex}. (c) and (g) Representative simulation snapshots of the transition state for the direct and indirect mechanism. (d) and (h) Distribution of transition times $p(\tau)$ for the direct and indirect exchange pathways.

© Author(s) 2021

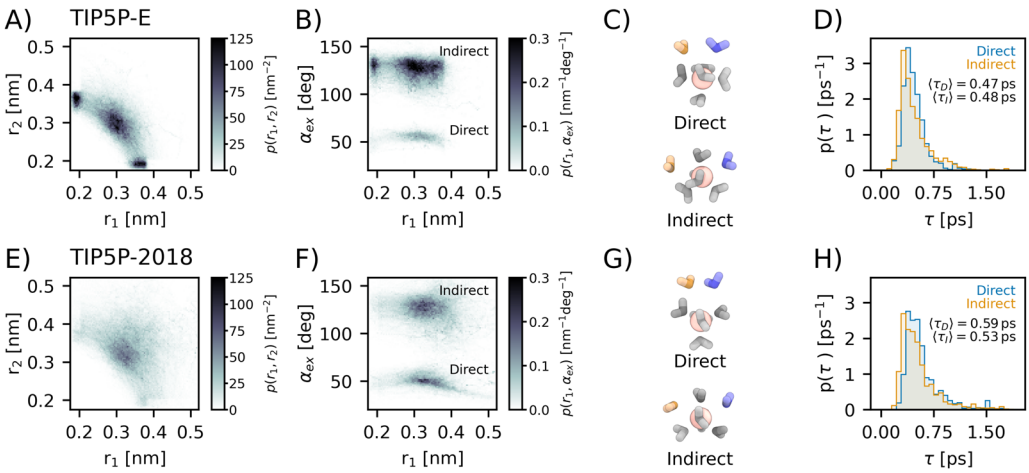

FIG. 4. Water exchange with the five-site water models TIP5P-E (top) and TIP5P/2018 (bottom). (a) and (e) Probability distribution function $p(r_1, r_2)$ along the transition pathways in dependence of the distances r_1 and r_2. (b) and (f) Probability distribution function $p(r_1, \alpha_{ex})$ in dependence of r_1 and the exchange angle α_{ex}. (c) and (g) Representative simulation snapshots of the transition state for the direct and indirect mechanism. (d) and (h) Distribution of transition times $p(\tau)$ for the direct and indirect exchange pathways.

Interchange associative pathways for polarizable and long-ranged force fields

Interestingly, an interchange associative exchange mechanism is observed with the polarizable AMOEBA force field and with the recently developed non-polarizable microMg parameters. The distributions of exchange distances along reactive pathways [Figs. 5(a) and 5(b) and Figs. 5(e) and 5(f)] show that the exchange takes place inside the first hydration shell (Fig. S1) and the distances in the transition state are only slightly larger compared to their equilibrium values (Table I). Similar to the dissociative pathways, direct and indirect exchanges are observed. Here, water molecules exchange in an angle of ~70° and 137° for direct and indirect paths, respectively. With seven water molecules in the inner shell, the transition state resembles a pentagonal bipyramidal geometry [Figs. 5(c) and 5(g)]. Consequently, the exchange angle is approximately a multiple of the central 72° angle. Considering the permutation invariance of solvent molecules, the transition states of direct and indirect reactions become virtually indistinguishable.

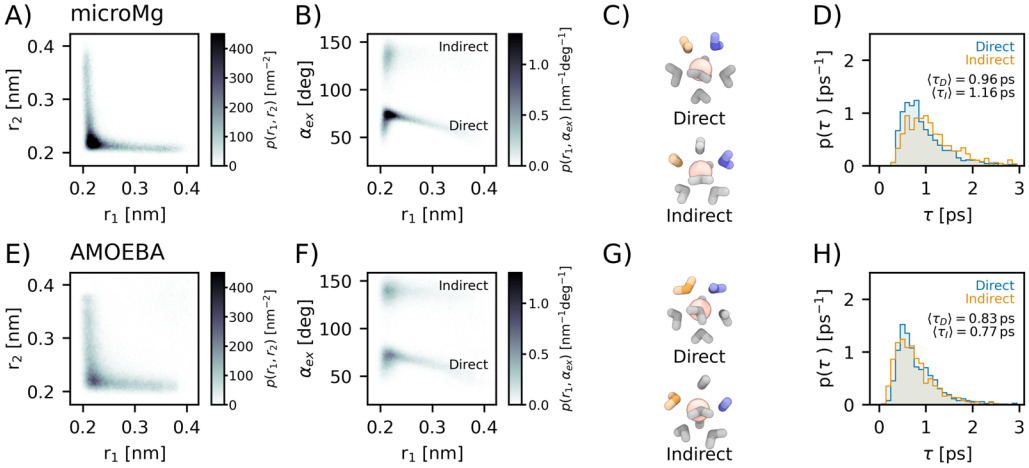

FIG. 5. Water exchange with the microMg parameters and TIP3P (top) and with the polarizable AMOEBA force field (bottom). (a) and (e) Probability distribution function $p(r_1, r_2)$ along the transition pathways in dependence of the distances r_1 and r_2. (b) and (f) Probability distribution function $p(r_1, \alpha_{ex})$ in dependence of r_1 and the exchange angle α_{ex}. (c) and (g) Representative simulation snapshots of the transition state for the direct and indirect mechanism. (d) and (h) Distribution of transition times $p(\tau)$ for the direct and indirect exchange pathways.

© Author(s) 2021

TABLE II. Water exchange rates: the exchange mechanism and water exchange rate k for different non-polarizable and polarizable force fields from the literature in comparison to the experimental results.

	Mechanism	k (s^{-1})
Mg^{2+}[12] in TIP3P	I_d	24.0 ± 8.8
microMg[13] in TIP3P	I_a	$8.0 \pm 1.2 \cdot 10^5$
AMOEBA[10,27]	I_a	$0.5 \cdot 10^9$
Expt.[6–8]	D, I_d	$5.3 \cdot 10^5$

The reason for the crossover from dissociative to associative mechanism is the range of the atomistic Mg^{2+}–water interaction potential of different force fields. Due to their high charge density, Mg^{2+} ions polarize their environment strongly. Consequently, charge-induced dipole interactions and charge transfer can become significant and render the Mg^{2+}–water interactions more attractive and long-ranged. The AMOEBA force field takes some of these many-body quantum effects into account explicitly while the microMg parameters account for them implicitly. In both cases, the Mg^{2+}–water interaction potentials are more long-ranged compared to standard force field parameters and have a non-vanishing attractive contribution at the edge of the first hydration shell (Fig. S2). Consequently, in the transition state, the exchanging water molecules have considerable interactions with the Mg^{2+} ion leading to the observed I_a mechanism. By contrast, for the more short-ranged interaction potential in the Mamatkulov Mg^{2+} force field, the interactions of the entering and leaving water molecules with Mg^{2+} are almost negligible.

The crossover from interchange dissociative to associative also affects the exchange rate (Table II). For the standard Mg^{2+} force field in combination with TIP3P water, the rate constant is $k = 24.0 \pm 8.8$ s^{-1}[12] and significantly lower than the experimental result ($k = 5.3 \cdot 10^5$ s^{-1}[6]). With the microMg parameters, the rate constant is $k = 8.0 \pm 1.2 \cdot 10^5$ s^{-1} and closely matches the experimental value.[13] The polarizable AMOEBA force field yields the highest rate $k = 0.5 \cdot 10^9$ s^{-1}[10,27] and significantly overestimates the experimental result.

CONCLUSION

Water exchange between the hydration shells of Mg^{2+} is essential for a large variety of physiological processes. In order to correctly capture the exchange dynamics in all-atom molecular dynamics simulations, accurate force fields are required. To ease the choice of the force field, we have systematically investigated the influence of different water models and Mg^{2+} force fields on the mechanism of water exchange. In particular, we have used transition path sampling as a particularly powerful sampling strategy to provide unbiased insights into the kinetic pathways and to cover the long timescales involved in water exchange.

In all cases, water exchange can occur either via an indirect or direct exchange pathway (exchanging molecules occupy different/same position on the water octahedron) without stable intermediates. This provides further evidence that the I_d mechanism is dominant while dissociative (D) pathways with a stable, reduced coordination intermediates can be excluded, in agreement with quantum mechanical calculations in the gas phase.[42] In addition, a crossover from an interchange dissociative (I_d) to an associative (I_a) reaction mechanism is observed dependent on the range of the Mg^{2+}–water interaction potential of the respective force field.

No force field combination tested in our current work is able to simultaneously reproduce the experimentally observed I_d mechanism and the rate of water exchange. Standard non-polarizable Mg^{2+} force fields in combination with the commonly used rigid water models yield the I_d mechanism in agreement with the experimental results but significantly underestimate the exchange rate.[12,13,19,20] The microMg parameters[13] yield close agreement with the experimental rate but follow the I_a mechanism in contrast to the experimental results. Finally, the polarizable AMOEBA force field[28,29] significantly overestimates the experimental rate and yields the I_a mechanism.

Consequently, the microMg force field parameters[13] should be used in bimolecular simulations addressing the binding kinetics and the Mamatkulov Mg^{2+} parameters[20] when addressing the mechanism of ligand exchange reactions. The applicability of the polarizable AMOEBA force field is clearly limited. However, models with variable polarizability[10] depending on the distance between Mg^{2+} and water or the application of scaled charge force fields for Mg^{2+}[48,49] might improve the agreement with the experimental results.

In any case, the impact of the water model and ionic force field must be explored in more detail in order to develop a more accurate description. In particular, designing an experiment that could probe water exchange pathways directly would be an invaluable contribution to the field. Alternatively, *ab initio* QM/MM molecular dynamics simulations[11] at high levels of accuracy could provide further insights and a step toward improved models for biomolecular simulations.

SUPPLEMENTARY MATERIAL

See the supplementary material for further discussion of the radial distribution function and the Mg^{2+}–water interaction potentials.

ACKNOWLEDGMENTS

This work was funded by the Deutsche Forschungsgemeinschaft (DFG, German Research Foundation), the Emmy Noether program (Grant No. 315221747). LOEWE CSC and GOETHE HLR are acknowledged for supercomputing access.

DATA AVAILABILITY

The data that support the findings of this study are available from the corresponding author upon reasonable request.

REFERENCES

[1] P. L. Geissler, C. Dellago, and D. Chandler, J. Phys. Chem. B **103**, 3706–3710 (1999).
[2] G. Schwaab, F. Sebastiani, and M. Havenith, Angew. Chem., Int. Ed. **58**, 3000–3013 (2018).
[3] A. Pyle, J. Biol. Inorg. Chem. **7**, 679–690 (2002).
[4] R. K. O. Sigel and A. M. Pyle, Chem. Rev. **107**, 97–113 (2007).

© Author(s) 2021

[5]J. Ostmeyer, S. Chakrapani, A. C. Pan, E. Perozo, and B. Roux, Nature **501**, 121–124 (2013).
[6]J. Neely and R. Connick, J. Am. Chem. Soc. **92**, 3476–3478 (1970).
[7]L. Helm and A. E. Merbach, Coord. Chem. Rev. **187**, 151–181 (1999).
[8]A. Bleuzen, P.-A. Pittet, L. Helm, and A. E. Merbach, Magn. Reson. Chem. **35**, 765–773 (1997).
[9]F. P. Rotzinger, J. Am. Chem. Soc. **118**, 6760–6766 (1996).
[10]I. V. Kurnikov and M. Kurnikova, J. Phys. Chem. B **119**, 10275–10286 (2015).
[11]A. Tongraar and B. M. Rode, Chem. Phys. Lett. **409**, 304–309 (2005).
[12]N. Schwierz, J. Chem. Phys. **152**, 224106 (2020).
[13]K. K. Grotz, S. Cruz-León, and N. Schwierz, J. Chem. Theory Comput. **17**, 2530–2540 (2021).
[14]N. F. A. van der Vegt, K. Haldrup, S. Roke, J. Zheng, M. Lund, and H. J. Bakker, J. Chem. Rev. **116**, 7626–7641 (2016).
[15]S. Funkner, G. Niehues, D. A. Schmidt, M. Heyden, G. Schwaab, K. M. Callahan, D. J. Tobias, and M. Havenith, J. Am. Chem. Soc. **134**, 1030–1035 (2012).
[16]P. K. Gupta, P. Schienbein, J. Daru, and D. Marx, J. Phys. Chem. Lett. **10**, 393–398 (2019).
[17]C. H. Langford and H. B. Gray, *Ligand Substitution Processes* (W. A. Benjamin, 1965).
[18]R. van Eldik, *Inorganic High Pressure Chemistry: Kinetics and Mechanisms* (Elsevier, Amsterdam, 1986).
[19]M. T. Panteva, G. M. Giambaşu, and D. M. York, J. Comput. Chem. **36**, 970–982 (2015).
[20]S. Mamatkulov and N. Schwierz, J. Chem. Phys. **148**, 074504 (2018).
[21]B. Hess, C. Kutzner, D. van der Spoel, and E. Lindahl, J. Chem. Theory Comput. **4**, 435–447 (2008).
[22]G. Bussi, D. Donadio, and M. Parrinello, J. Chem. Phys. **126**, 014101 (2007).
[23]P. Eastman, J. Swails, J. D. Chodera, R. T. McGibbon, Y. Zhao, K. A. Beauchamp, L.-P. Wang, A. C. Simmonett, M. P. Harrigan, C. D. Stern, R. P. Wiewiora, B. R. Brooks, and V. S. Pande, PLoS Comput. Biol. **13**, e1005659 (2017).
[24]D. A. Sivak, J. D. Chodera, and G. E. Crooks, J. Phys. Chem. B **118**, 6466–6474 (2014).
[25]A. Rizzi *et al.* (2020). "Choderalab/openmmtools: 0.20.0 - Periodic nonequilibrium integrator," Zenodo. https://doi.org/10.5281/zenodo.3930570.
[26]D. Jiao, C. King, A. Grossfield, T. A. Darden, and P. Ren, J. Phys. Chem. B **110**, 18553–18559 (2006).
[27]J. C. Wu, J.-P. Piquemal, R. Chaudret, P. Reinhardt, and P. Ren, J. Chem. Theory Comput. **6**, 2059–2070 (2010).
[28]J. W. Ponder, C. Wu, P. Ren, V. S. Pande, J. D. Chodera, M. J. Schnieders, I. Haque, D. L. Mobley, D. S. Lambrecht, R. A. DiStasio, M. Head-Gordon, G. N. I. Clark, M. E. Johnson, and T. Head-Gordon, J. Phys. Chem. B **114**, 2549–2564 (2010).
[29]P. Ren and J. W. Ponder, J. Phys. Chem. B **107**, 5933–5947 (2003).
[30]H. J. C. Berendsen, J. R. Grigera, and T. P. Straatsma, J. Phys. Chem. **91**, 6269–6271 (1987).
[31]W. L. Jorgensen, J. Chandrasekhar, J. D. Madura, R. W. Impey, and M. L. Klein, J. Chem. Phys. **79**, 926–935 (1983).
[32]J. L. F. Abascal and C. Vega, J. Chem. Phys. **123**, 234505 (2005).
[33]S. Piana, A. G. Donchev, P. Robustelli, and D. E. Shaw, J. Phys. Chem. B **119**, 5113–5123 (2015).
[34]C. Vega and J. L. F. Abascal, Phys. Chem. Chem. Phys. **13**, 19663–19688 (2011).
[35]S. W. Rick, J. Chem. Phys. **120**, 6085–6093 (2004).
[36]Y. Khalak, B. Baumeier, and M. Karttunen, J. Chem. Phys. **149**, 224507 (2018).
[37]M. W. Mahoney and W. L. Jorgensen, J. Chem. Phys. **112**, 8910–8922 (2000).
[38]D. W. H. Swenson, J.-H. Prinz, F. Noe, J. D. Chodera, and P. G. Bolhuis, J. Chem. Theory Comput. **15**, 813–836 (2019).
[39]D. W. H. Swenson, J.-H. Prinz, F. Noe, J. D. Chodera, and P. G. Bolhuis, J. Chem. Theory Comput. **15**, 837–856 (2019).
[40]G. A. Tribello, M. Bonomi, D. Branduardi, C. Camilloni, and G. Bussi, Comput. Phys. Commun. **185**, 604–613 (2014).
[41]H. Jung, K.-i. Okazaki, and G. Hummer, J. Chem. Phys. **147**, 152716 (2017).
[42]Z. Qian, H. Feng, C. Wang, and J. Chen, Inorg. Chim. Acta **363**, 3627–3631 (2010).
[43]S. Decherchi and W. Rocchia, PLoS One **8**, e59744 (2013).
[44]C. Dellago, P. G. Bolhuis, F. S. Csajka, and D. Chandler, J. Chem. Phys. **108**, 1964–1977 (1998).
[45]P. G. Bolhuis, D. Chandler, C. Dellago, and P. L. Geissler, Annu. Rev. Phys. Chem. **53**, 291–318 (2002).
[46]P. G. Bolhuis and C. Dellago, in *Reviews in Computational Chemistry*, Trajectory-Based Rare Events Simulations, edited by K. B. Lipkowitz (Wiley, 2010), Vol. 27.
[47]D. J. Huggins, J. Chem. Phys. **136**, 064518 (2012).
[48]I. M. Zeron, J. L. F. Abascal, and C. Vega, J. Chem. Phys. **151**, 134504 (2019).
[49]I. M. Zeron, M. A. Gonzalez, E. Errani, C. Vega, and J. L. F. Abascal, J. Chem. Theory Comput. **17**, 1715–1725 (2021).

© Author(s) 2021